DOI: 10.1002/asia.201300570

Ligand-Functionalization of BPEI-Coated YVO_4:Bi^{3+},Eu^{3+} Nanophosphors for Tumor-Cell-Targeted Imaging Applications**

Yi-Chin Chen,[a] Sheng-Cih Huang,[b] Yu-Kuo Wang,[b] Yuan-Ting Liu,[c] Tung-Kung Wu,[b] and Teng-Ming Chen*[a]

Abstract: In this study, surface-functionalized, branched polyethylenimine (BPEI)-modified YVO_4:Bi^{3+},Eu^{3+} nanocrystals (NCs) were successfully synthesized by a simple, rapid, solvent-free hydrothermal method. The BPEI-coated YVO_4:Bi^{3+},Eu^{3+} NCs with high crystallinity show broad-band excitation in the $\lambda = 250$ to 400 nm near-ultraviolet (NUV) region and exhibit a sharp-line emission band centered at $\lambda = 619$ nm under excitation at $\lambda = 350$ nm. The surface amino groups contributed by the capping agent, BPEI, not only improve the dispersibility and water/buffer stability of the BPEI-coated YVO_4:Bi^{3+},Eu^{3+} NCs, but also provide a capability for specifically targeted biomolecule conjugation. Folic acid (FA) and epidermal growth factor (EGF) were further attached to the BPEI-coated YVO_4:Bi^{3+},Eu^{3+} NCs and exhibited effective positioning of fluorescent NCs toward the targeted folate receptor overexpressed in HeLa cells or EGFR overexpressed in A431 cells with low cytotoxicity. These results demonstrate that the ligand-functionalized, BPEI-coated YVO_4:Bi^{3+},Eu^{3+} NCs show great potential as a new-generation biological luminescent bioprobe for bioimaging applications. Moreover, the unique luminescence properties of BPEI-coated YVO_4:Bi^{3+},Eu^{3+} NCs show potential to combine with a UVA photosensitizing drug to produce both detective and therapeutic effects for human skin cancer therapy.

Keywords: biological activity · imaging agents · lanthanides · nanostructures · polymers

Introduction

Cancer is one of the top ten causes of death worldwide. The survival rate of cancer has not significantly improved in the past two decades. Fortunately, with regard to many cancers, there is a high possibility for important biotechnology for cancer diagnostic procedures and cancer prevention.[1] Recently, a number of novel composite nanomaterials have been investigated and developed for biological applications, including drug and gene delivery,[2] biosensing,[3] and bioimaging.[4] For instance, luminescent semiconductor quantum dots (QDs) are highly effective for cellular and animal imaging.[5] Nevertheless, it is generally known that QDs exhibit problematic weak photostability, broad emission bands, optical blinking, short luminescence lifetimes, short light penetration depths, surface ligand incompatibility, and the presence of strong background fluorescence in certain analyzed systems. In addition, the surface oxidation of QDs through various biochemical pathways leads to the release of heavy metals from the surfaces of the QDs; thus, inducing cell death and greatly limiting their practical applications.[6]

Compared with QDs, lanthanide-doped inorganic nanoparticles maintain high chemical and photochemical stability, tunable emission color,[7] long luminescence lifetimes[8] (from μs to several ms), low photobleaching potentials, and low biotoxicity; all of which make them capable of promoting detection sensitivity for biological labeling and imaging applications.[9] Recently, several fluorescence probes consisting of lanthanide-doped fluoride and oxide nanocrystals (NCs), such as $NaYF_4$:Yb^{3+},Er^{3+} and Y_2O_3:Tb^{3+}, were effective for biological detection.[10] In particular, upconversion nanophosphors (UCPs) have been considered as a new generation of luminescent probes for bioimaging applications.[11] UCPs present several advantages, including high sensitivity, minimal photobleaching, and high penetration depths. Most of all, the IR excitation is less harmful to living cells and small animals. However, lower upconversion efficiency (less than 1%) compared with downconversion nanophosphors limits their applications in bioimaging and biosensing applications.[12]

[a] Y.-C. Chen, Prof. Dr. T.-M. Chen
Department of Applied Chemistry and Institute of Molecular Science
National Chiao Tung University, Science Building 2
1001 Ta Hsueh Road, Hsinchu, 300 (Taiwan)
Fax: (+886) 3-5723764
E-mail: tmchen@mail.nctu.edu.tw

[b] S.-C. Huang, Dr. Y.-K. Wang, Prof. Dr. T.-K. Wu
Department of Biological Science and Technology
National Chiao Tung University, Tin Ka Ping Building
1001 Ta Hsueh Road, Hsinchu, 300 (Taiwan)

[c] Dr. Y.-T. Liu
Department of Applied Chemistry and Institute of Molecular Science
National Chiao Tung University, Tin Ka Ping Building
1001 Ta Hsueh Road, Hsinchu, 300 (Taiwan)

[**] BPEI = branched polyethylenimine.

Supporting information for this article is available on the WWW under http://dx.doi.org/10.1002/asia.201300570.

Yttrium orthovanadate doped with lanthanides (YVO_4:Ln) is a well-known optical material with a variety of emitting colors and high luminescence efficiency compared with fluorides and other lanthanide-doped oxide NCs.[13] It has been reported that the edge of YVO_4: Eu^{3+} excitation peak shifts toward longer wavelengths from $\lambda = 350$ to 400 nm upon doping with Bi^{3+} ions.[14] YVO_4:Bi^{3+},Eu^{3+} also shows some attractive features, including sharp emission peaks, large stoke shifts, high luminescence efficiency, and long lifetimes. In this study, we have designed and prepared branched polyethylenimine (BPEI)-coated YVO_4:Bi^{3+},Eu^{3+} NCs through a simplistic, cost-effective, and environmental friendly synthetic route. The structure, morphology, and luminescence properties of BPEI-coated YVO_4:Bi^{3+},Eu^{3+} NCs were investigated in detail. Moreover, we have also successfully demonstrated the use of the as-prepared BPEI-coated YVO_4:Bi^{3+},Eu^{3+} NCs as fluorescent labels for in vitro bioimaging and confirmed their relative nontoxicity.

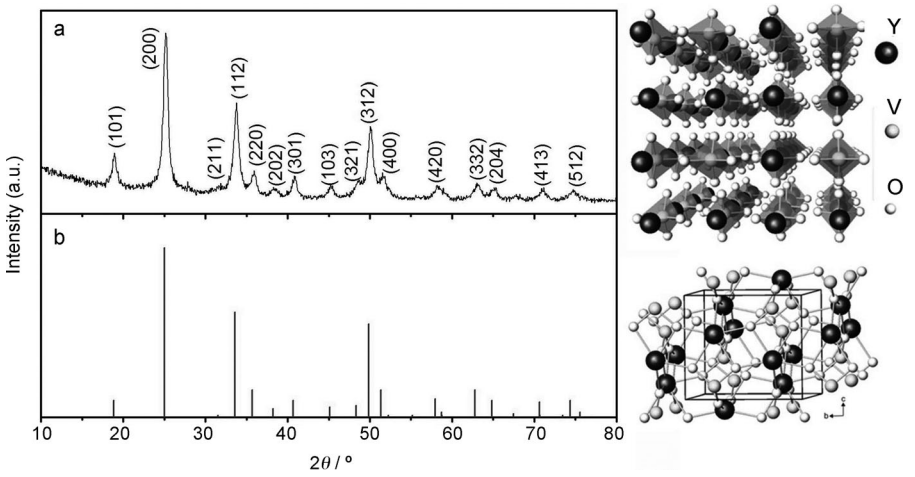

Figure 1. XRD patterns of YVO_4:Bi^{3+},Eu^{3+} NCs prepared by the hydrothermal method (a) and the standard data for tetragonal YVO_4 (ICSD No.78074) used as a reference (b).

Results and Discussion

The BPEI-modified YVO_4:Bi^{3+},Eu^{3+} NCs were synthesized by using a facile one-pot hydrothermal method. The hydrothermal synthesis can be carried out in a water-based system and at a relatively low reaction temperature (160–220 °C) and short reaction time (2 h) through an environmentally friendly approach. In this experiment, we altered the sequence and the rate of adding the materials to improve reactivity. In addition, an autoclave reactor equipped with a magnetic stirrer, with an independent heating system, provides a more homogeneous and uniform heating reaction process than a traditional autoclave reactor. The well-controlled synthetic procedure can produce uniform NCs with high-quality properties and decrease the energy consumption efficiency during the synthetic process. Figure 1 shows the XRD data of the as-synthesized YVO_4:Bi^{3+},Eu^{3+} NCs coated with BPEI polymer. All of the diffraction peaks observed from the sample can be readily indexed to a tetragonal phase of a single crystal of YVO_4 (ICSD no. 78074) with space group $I4_1/amd$. The result shows a single phase with no unidentified diffraction peaks from impurities. In the crystal structure of YVO_4, there is only one crystallographically distinct site for the Y atoms. The Y^{3+} ions are eightfold coordinated to oxygen ions and located in a lattice site with D_{2d} symmetry. For the YVO_4:Bi^{3+},Eu^{3+} NCs, Y^{3+} ions are substituted by larger Bi^{3+} and Eu^{3+} ions; thus, the XRD peaks shift toward the lower-angle side because of the increase in interplanar spacing. The broadening diffraction peaks of the YVO_4:Bi^{3+},Eu^{3+} NCs prepared by the hydrothermal method indicate a decrease of the crystalline particle size. The average particle size, as determined using the Debye–Scherrer formula,[15] is calculated to be 19.73 nm.

The BPEI polymer is a thermally stable, hydrophilic polymer with primary, secondary, and tertiary amino groups. During the hydrothermal reaction process, the BPEI polymer was used as a chelating agent and a structure-regulating agent to control the particle size and morphology of the obtained NCs. The nitrogen atoms in the main and side chains of BPEI can serve as electron donors to chelate lanthanide ions and form complexes with rare-earth ions through coordination. The crystal seeds were recrystallized into single crystals during hydrothermal treatment and the BPEI molecules can be tightly bound to the NC surface.[10a] From a TEM image (Figure 2a), the sample exhibits nearly spheri-

Abstract in Chinese:

本研究利用簡單、快速的水熱法製備奈米級釩酸釓螢光體，並以親水性高分子聚合物 BPEI 作為分散劑輔助反應，可得到純相、結晶性佳、分散性良好奈米級釩酸釓螢光體。親水性高分子 BPEI 可對奈米螢光體表面進行改質，使其表面帶有胺基而能均勻分散於水溶液中，並可利用此胺基與生物分子鍵結，應用於生物檢測及生物顯影。藉由摻雜稀土離子 Bi^{3+}及 Eu^{3+}之間的能量轉移可使 YVO_4:Bi^{3+}, Eu^{3+}螢光體在近紫外光的激發下放射 619 nm 的紅光。此光學特性顯示奈米級 YVO_4:Bi^{3+}, Eu^{3+} 螢光體具有應用於 PUVA 光療之潛能。

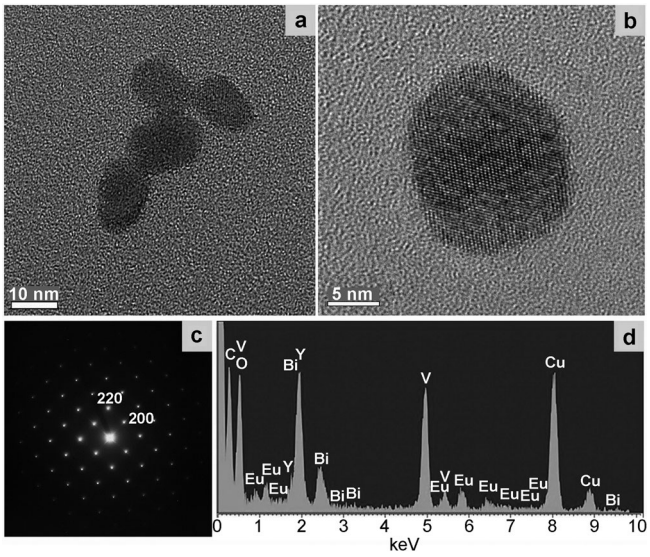

Figure 2. Crystal morphology and compositions of BPEI-coated YVO_4:Bi^{3+},Eu^{3+} NCs: a) TEM image, b) a high-resolution (HR) TEM image, c) a selected-area electron diffraction (SAED) pattern, and d) an energy-dispersive X-ray (EDX) spectrum.

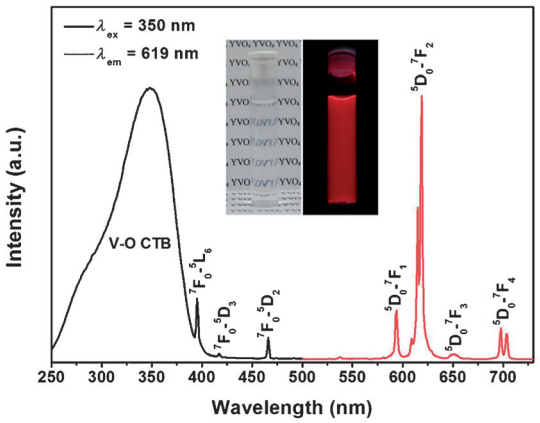

Figure 3. Excitation and emission spectra of BPEI-coated YVO_4:Bi^{3+},Eu^{3+} NCs. The inset shows the luminescence of BPEI-coated YVO_4:Bi^{3+},Eu^{3+} NCs in deionized water (DIW) under daylight and near-ultraviolet (NUV) irradiation.

cal shapes and more than 90% of NCs are within the 13–38 nm size range. The average particle size is (19.36 ± 0.29) nm (random sample of 100 NCs). This result is consistent with the calculated average particle size from XRD and further confirmed by dynamic light scattering (DLS) analysis. Figure S1 in the Supporting Information shows that there is only one population within the 10–40 nm size range, and the major distribution is around 20 nm. In the HRTEM image (Figure 2b), the lattice fringes are clearly distinguishable and show high-order lattice ordering, which suggests the single-crystalline nature of the BPEI-coated YVO_4:Bi^{3+},Eu^{3+} crystalline nanoparticles. The composition of the obtained BPEI-coated YVO_4:Bi^{3+},Eu^{3+} NCs was confirmed by EDX analysis (Figure 2d), and only Y, V, Bi, Eu, and O elements were observed, as expected. The copper signal in the EDX spectrum originated from the copper grid used as a sample holder in the measurement. These results reveal that the obtained NCs exhibit high crystallinity and uniform morphology at a relatively low reaction temperature and short reaction time.

As shown in the excitation spectrum (Figure 3), the strong absorption band from $\lambda = 250$ to 300 nm centered at around $\lambda = 280$ nm (monitored by emission at $\lambda = 619$ nm) was due to charge transfer (CT) from the oxygen ligands to the central vanadium atom within the VO_4^{3-} group.[16] The absorption band is overlaid with the CT transition band of O^{2-}–Eu^{3+} at $\lambda \approx 260$ nm.[17] The excitation peak between $\lambda = 300$ and 400 nm originated from metal–metal CT transitions from the Bi^{3+} to the V^{5+} ion followed by energy transfer to Eu^{3+}.[18] The sharp excitation band at $\lambda = 395$ nm corresponds to the $^7F_0$–$^5L_6$ transition within the $4f^6$ configuration of the Eu^{3+} ions. The photoluminescence (PL) spectrum shows a typical linear feature for Eu^{3+} emission under excitation at $\lambda = 350$ nm, and the sharp emission peaks ranging from $\lambda = 580$ nm to 730 nm can be ascribed to radiative transitions from the $^5D_0$ level to the ^7F_J ($J = 1, 2, 3, 4$) level of the Eu^{3+} ion.[13a,18a] The BPEI-coated YVO_4:Bi^{3+},Eu^{3+} NCs can be well dispersed in distilled water and form a stable transparent colloidal solution without precipitation over a period of several months. As shown in the inset of Figure 3, strong red light contributed from the most intensive emission peak at $\lambda = 619$ nm can be observed under NUV light excitation. Compared with other rare-earth-doped oxide NCs, the excitation band of BPEI-coated YVO_4:Bi^{3+},Eu^{3+} NCs extend to longer wavelengths; this provides a greater depth penetration to achieve long imaging depths in intact tissue. Moreover, the sharp emission feature gives clear imaging to allow distinction between the fluorescent signal and the typical biological autofluorescence background. This feature is an important advantage for bioimaging applications.

Photochemotherapy is widely used for the treatment of nonmalignant hyperproliferative skin conditions and cancers, such as vitiligo, psoriasis, atopic dermatitis (AD), scleroderma, and T-cell lymphoma (CTCL).[19] The most common used treatment, psoralen plus ultraviolet light therapy (PUVA), is combined with a photosensitizing drug to make the skin more sensitive to UV light and produce a therapeutic effect that neither drug nor radiation alone can achieve.[20] However, the photosensitizers employed are often not specific for the target tissue, which not only decreases the therapeutic effect, but also increases the risk of skin cancer owing to long-term use of PUVA therapy. As a result, it is important to develop a UVA photosensitizer that can recognize target tissues specifically to improve the therapeutic activity. The strong UV light absorption of BPEI-coated YVO_4:Bi^{3+},Eu^{3+} NCs can increase UV light absorption to make the target tissue more sensitive to UV light and improve the therapeutic activity. In addition, the long-wavelength red emission can penetrate the skin and make it easier to determine the location of cancer cells. Based on the above unique optical properties of BPEI-

coated YVO_4:Bi^{3+},Eu^{3+} NCs, we assumed that surface-functionalized BPEI-coated YVO_4:Bi^{3+},Eu^{3+} NCs would show great potential as a photosensitizer drug carrier to produce both detective and therapeutic effects for human skin cancer therapy.

Antibodies,[21] folic acid (FA)[2b,10b,22] peptides,[4b,23] and other small molecular ligands are modified on the surfaces of nanoparticles; this validates the specific targeting of cancer cells. A glycosylphosphatidylinositol (GPI)-anchored membrane protein, folate-receptors (FR), was found to be overexpressed in a wide variety of human tumors, while FA is a high-affinity ligand for FR. Previous studies have shown that folate conjugates selectively bind to the surface of the receptor-bearing tumor cell to trigger receptor-mediated endocytosis (Figure 4).[24]

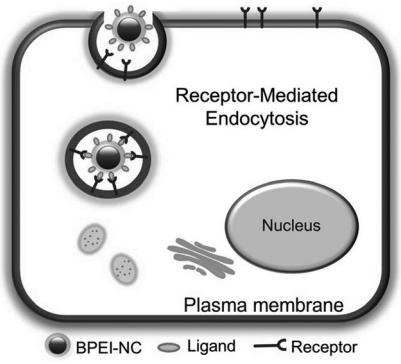

Figure 4. The cellular uptake of ligand-functionalized NCs into a human cancer cell through the receptor-mediated endocytosis mechanism.

To explore the capability of ligand-functionalized, BPEI-coated YVO_4:Bi^{3+},Eu^{3+} NCs for cancer cell targeted imaging applications, FA-conjugated, BPEI-coated YVO_4:Bi^{3+},Eu^{3+} NCs were designed and studied. To conjugate FA to BPEI-coated YVO_4:Bi^{3+},Eu^{3+} NCs, the ethyl(dimethylaminopropyl)carbodiimide (EDC)/*N*-hydroxysuccinimide (NHS) coupling reaction was applied. The amino groups on the NC surface provided from BPEI can be activated by EDC to form an amine-reactive intermediate. Sulfo-NHS converts the intermediate into an amine-reactive sulfo-NHS ester compound, which then covalently conjugates to the carboxyl groups of FA through a two-step cross-linking process. The conjugation of FA to BPEI-coated YVO_4:Bi^{3+},Eu^{3+} NCs was confirmed by FTIR spectroscopy. As shown in Figure 5, the BPEI-coated YVO_4:Bi^{3+},Eu^{3+} NCs show a characteristic V–O vibration band from the VO_4^{3-} group at $\tilde{\nu}=810\,cm^{-1}$; the weak absorption band at $\tilde{\nu}=451\,cm^{-1}$ is attributed to the Y–O stretching vibrations of the host lattice. The broad band at $\tilde{\nu}=3407\,cm^{-1}$ corresponds to the O–H or N–H stretching vibrations, whereas the bands at $\tilde{\nu}=$ 1633 and 1385 cm^{-1} are related to the bending vibrations of the N–H bond in the BPEI polymer. The weak bands at $\tilde{\nu}=$ 2923 and 2849 cm^{-1} can be assigned to the asymmetric and symmetric stretching vibrations of $-CH_2$ in the BPEI polymer. These results may indicate possible coating or partial

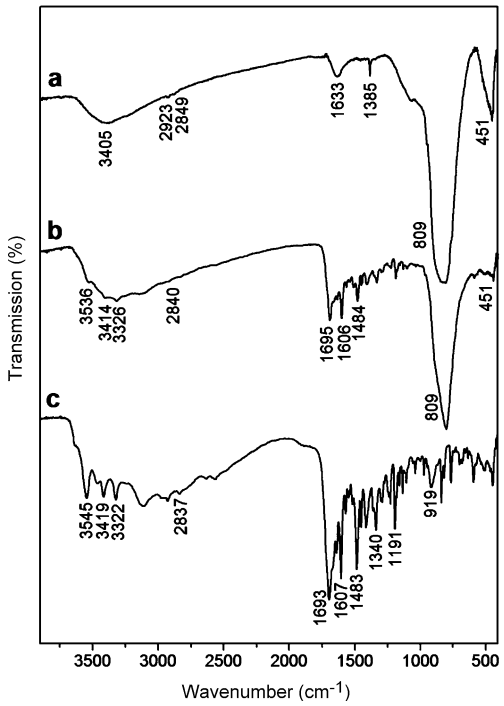

Figure 5. FTIR spectra of a) BPEI-coated YVO_4:Bi^{3+},Eu^{3+} NCs; b) FA conjugated with BPEI-YVO_4:Bi^{3+},Eu^{3+} NCs; and c) FA.

coating of BPEI polymer on the NC surface. Further characterization is required to determine whether the NC surface is well coated with BPEI polymer. Compared with the bare BPEI-coated YVO_4:Bi^{3+},Eu^{3+} NCs, the FTIR spectrum of FA–BPEI–YVO_4:Bi^{3+},Eu^{3+} NCs exhibits characteristic absorption peaks of FA at $\tilde{\nu}=1606\,cm^{-1}$ that are attributed to conjugated double absorption of benzene at $\tilde{\nu}=1695$ (ester bond) and 1484 cm^{-1} (heteroring, conjugated double bond). In addition, the absorption bands at $\tilde{\nu}=3536$, 3414, and 3326 cm^{-1} correspond to the amide NH and NH_2 stretching vibrations of the folate conjugate. These results confirm the successful conjugation of FA with BPEI-coated YVO_4:Bi^{3+}, Eu^{3+} NCs.

The BPEI polymer shows high positive charge density provided by the amino groups and high buffering capacity within a wide range of pH conditions.[25] This is of great importance for the prevention of aggregation under physiological conditions. Furthermore, the net positive charge can facilitate cellular uptake and cell-binding affinity in several human cell lines.[10c] Theoretically, it may result in nonspecific binding to cells by electrostatic interactions between positively charged NCs and negatively charged plasma membranes of cells. However, a number of studies have reported that proper grafting of PEI with targeting ligands can efficiently internalize NCs into the target cells, which are distinguishable from the nontarget cells.[26] Human cervical carcinoma cell line (HeLa) cells, which express abundant FRs on the cell membrane, were used as a model system for in vitro bioimaging. In this experiment, HeLa cells were incubated with FA–BPEI–YVO_4:Bi^{3+},Eu^{3+} NCs (0.5 mg mL^{-1}) for 4 h

at 37 °C. No background fluorescence could be observed under UV light excitation in the control reaction, in which HeLa cells were incubated without NC. Bare BPEI-coated YVO_4:Bi^{3+},Eu^{3+} NCs were incubated with HeLa cells under the same experimental conditions as the negative control. As shown in Figure S2 in the Supporting Information, no red emission could be observed, although some aggregated NCs were randomly distributed in the culture dishes. Compared with the negative control, large amounts of FA–BPEI–YVO_4:Bi^{3+},Eu^{3+} NCs were specifically attached to the cell membrane of HeLa cells that exhibited strong red emission under UV light excitation in the dark-field image (Figure 6). In addition, the fluorescence intensity did not show clear photobleaching phenomena under continuous excitation during the observation period. In our previous work, the decay lifetime of BPEI-coated YVO_4:Bi^{3+},Eu^{3+} was about 751.59 μs, in accordance with the literature.[27] We assume that the long luminescence lifetime and PL stability of BPEI-coated YVO_4:Bi^{3+},Eu^{3+} can overcome the detective limitations of organic dyes. The optical stability has also been discussed in other nanophosphors.[10e,28] The overlay of bright- and dark-field images (Figure 6c) further demonstrated that the red-emitting NCs were specifically located on the surface of the cancer cell.

The targeting efficiency may be influenced by ligand numbers, the site of ligand coupling, and interactions between the ligand and NCs. Although FA-modified, BPEI-coated YVO_4:Bi^{3+},Eu^{3+} NCs can specifically interact with FRs on the membrane of the cancer cell, FA decomposed rapidly in the presence of light during the FA–NC cross-linking reaction. The decreased FA–NC cross-linking efficiency might further influence the sensitivity of cancer cell detection. To improve the sensitivity of cancer cell detection, another particular ligand, epidermal growth factor (EGF), which is a low-molecular-weight polypeptide that acts as a ligand molecule for the epidermal growth factor receptor (EGFR), was also conjugated with BPEI-coated YVO_4:Bi^{3+},Eu^{3+} NCs to illustrate the specific recognition and interaction with cancer cells. The EGF–EGFR interaction is rapid and stable, which provides a rational approach for use in cancer imaging and treatment.[4b,23b,29] MALDI-TOF mass spectrometry analysis is a valuable tool for the analysis of biomolecules owing to the advantages of fast data collection, high sensitivity, and low sample volume, as well as providing good, qualitative data.[30]

The successful conjugation of EGF with BPEI-coated YVO_4:Bi^{3+},Eu^{3+} NCs was confirmed by MALDI-TOF MS analysis, as shown in Figure 7. The bottom spectrum in Figure 7a shows that no clear signal could be detected in the sample of bare BPEI-coated YVO_4:Bi^{3+},Eu^{3+} NCs. Conversely, a strong signal could be observed in the sample of EGF-BPEI-YVO_4 NCs at m/z 6345.4 (Figure 7a, top spectrum), which corresponds to the molecular weight of the EGF protein (≈6216 Da with 53 amino acid residues). To ensure reliable and accurate identification of EGF conjugation, defined peptide fragments generated by trypsin digestion were subjected to MALDI-TOF MS/MS analysis. The specific peptide fragment containing eight amino acid residues (Asp-Leu-Lys-Trp-Trp-Glu-Leu-Arg) was identified, derived from the C-terminal fragment sequence of the EGF protein (Figure 7b).

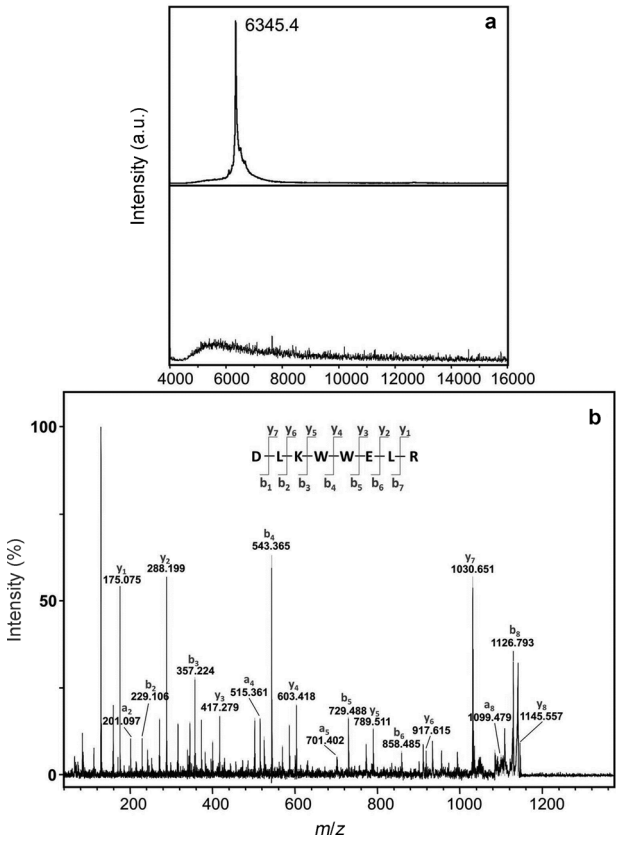

Figure 7. MALDI-TOF mass spectra of EGF-BPEI-YVO_4 NCs a) before and b) after being digested by trypsin.

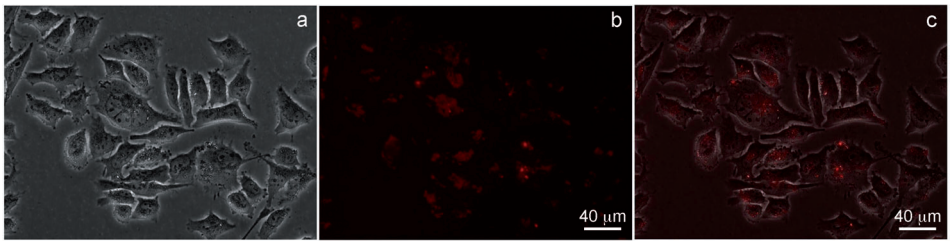

Figure 6. Fluorescent microscopy images showing the interaction of HeLa cells with FA–BPEI–YVO_4:Bi^{3+},Eu^{3+} NCs (0.5 mg mL^{-1}) for 4 h at 37 °C: a) bright field, b) dark field, and c) merged images.

The EGF-modified BPEI-coated YVO_4:Bi^{3+},Eu^{3+} NCs were incubated with the human epidermoid carcinoma cell line (A431) cells at different concentrations (0.06, 0.12, and 0.24 mg mL^{-1}). A431 cells

are typically used in studies of the cell cycle and cancer-associated cell signaling pathways because they express abnormally high levels of EGFR on the cell membrane. The fluorescent microscopy images of EGF-BPEI-YVO_4:Bi^{3+},Eu^{3+} NCs targeting A431 cells are displayed in Figure 8. The

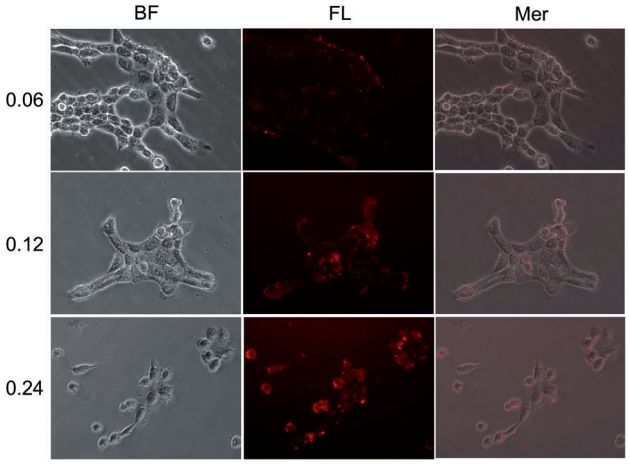

Figure 8. Fluorescent microscopy images of A431 cells incubated with BPEI-coated YVO_4:Bi^{3+},Eu^{3+} NCs modified with EGF at different concentrations (0.06, 0.12, and 0.24 mg mL^{-1}) for 2 h at 37 °C. BF = bright field, FL = fluorescence, and Mer = merged.

EGF-BPEI-YVO_4:Bi^{3+},Eu^{3+} NCs showed high-affinity targeting of A431 cells overexpressing EGFR, even at a low concentration (0.06 mg mL^{-1}) and short incubation time (2 h). Upon increasing the concentration of EGF-BPEI-YVO_4:Bi^{3+},Eu^{3+} NCs, the NCs showed concentration-dependent cellular uptake in A431 cells. In addition, A431 cells were also treated with bare BPEI-coated YVO_4:Bi^{3+},Eu^{3+} NCs under the same experimental conditions as those used for the negative control. As shown in Figure S2 in the Supporting Information, the weak red luminescence suggested that the nonspecific interaction of NCs with the A431 cell membrane was very weak. From these results, we propose that ligand-functionalized, BPEI-coated YVO_4:Bi^{3+},Eu^{3+} NCs can efficiently attach to cancer cells and generate sufficiently strong fluorescence for bioimaging purposes.

The cytotoxicity of BPEI-coated YVO_4:Bi^{3+},Eu^{3+} NCs was evaluated on A431 cells. A431 cells were treated with different concentrations (0.1, 0.2, and 0.5 mg mL^{-1}) of BPEI-coated YVO_4:Bi^{3+},Eu^{3+} NCs for 2–24 h to determine the cell viability relative to untreated cells by the 3-(4,5-dimethylthiazol-2-yl)-2,5-diphenyltetrazolium bromide (MTT) assay. Because the BPEI polymer exhibits severe cellular toxicity for the induction of cell apoptosis, it could be presumed that the BPEI-coated YVO_4:Bi^{3+},Eu^{3+} NCs may exhibit potential cytotoxicity derived from the surface BPEI coating. Fortunately, the MTT assay revealed that cytotoxicity was not apparent with 0.5 mg mL^{-1} BPEI-coated YVO_4:Bi^{3+},Eu^{3+} NCs, which was 10-fold higher than the concentration used in live-cell imaging (Figure 9). After increasing incubation time up to 24 h, no significant cellular

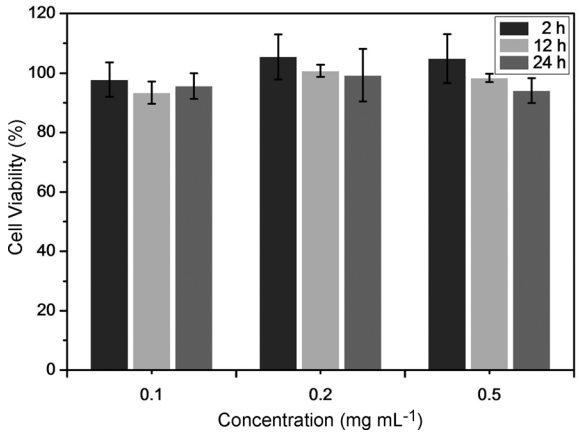

Figure 9. In vitro cell viability of A431 cells incubated with BPEI-YVO_4:Bi^{3+},Eu^{3+} NCs at different concentrations for periods ranging from 2 to 24 h. The viability of untreated cells was assumed to be 100 %.

toxicity was observed. Moreover, the fluorescent microscopy images in bright-field measurements taken after treatment with NCs confirmed that the cells were viable, and there were no evident regions of cell death. We assume that the amount of BPEI coating was controlled to decrease cytotoxicity, but sufficient for surface functionalization. Therefore, these data strongly suggest that surface-functionalized rare-earth-doped YVO_4:Bi^{3+},Eu^{3+} NCs can be considered to possess reasonably low cytotoxicity and are safe enough for cancer cell targeted imaging applications.

Conclusion

We have demonstrated that monodispersed BPEI-coated YVO_4:Bi^{3+}, Eu^{3+} NCs synthesized by a facile one-step hydrothermal method can be utilized as versatile luminescent probes for bioimaging applications. The water-based system provides a simple, rapid, solvent-free, and safe synthetic route for nanomaterial preparation. The resulting BPEI-coated YVO_4:Bi^{3+},Eu^{3+} NCs exhibited good water/buffer dispersibility and were not only biocompatible with cells, but also relatively nontoxic over reasonable incubation time periods and concentrations. The luminescence properties and specific tumor targeting efficiency were also investigated in this study. The obtained BPEI-coated YVO_4:Bi^{3+}, Eu^{3+} NCs showed a strong red luminescence ($\lambda = 619$ nm) under NUV excitation. The special spectroscopic properties of BPEI-coated YVO_4:Bi^{3+}, Eu^{3+} NCs exhibit potential as a bifunctional biomaterial for bioimaging and photochemotherapy applications. In vitro bioimaging results showed that ligand–NC conjugates could be specifically taken up by cancer cells, depending on the targeted ligands on the surface of the NCs, through a receptor-mediated endocytosis mechanism. The results showed that ligand-functionalized BPEI-coated YVO_4:Bi^{3+}, Eu^{3+} NCs had good detection sensitivity, even at a low concentration and a short incubation time. This strategy could be further extended to other lan-

thanide-doped luminescent nanomaterials to develop multicolor bioprobes for biodetection and drug-delivery applications.

Experimental Section

Preparation of BPEI-Coated YVO_4:Bi^{3+},Eu^{3+} NCs

BPEI-coated YVO_4:Bi^{3+},Eu^{3+} NCs were synthesized by a hydrothermal method. The required amounts of $Ln(NO_3)_3{\cdot}5H_2O$ (Ln = Y, Bi, and Eu) were dissolved in DIW (10 mL) and stirred at room temperature to afford a transparent solution (Y/Bi/Eu/V = 0.7:0.15:0.15:1). Then, BPEI solution was added to the mixture. The BPEI concentration of the final growth solution was 0.04 g mL^{-1}. In another vessel, NH_4VO_3 (1 mmol) was dissolved in a solution of sodium hydroxide (10 mL) at pH 12, and the aqueous solution was added dropwise to the mixture. A 0.5 M aqueous solution of NaOH was added dropwise to tune the final pH of the growth solution to 7. After stirring for 1 h at 80 °C, the obtained transparent solution was transferred into a 125 mL Teflon-lined magnetic stirrer autoclave system for hydrothermal treatment at 180 °C for 2 h with a slow heating rate of 3 °C min^{-1}. After cooling to room temperature, the products were collected by centrifugation (10 min at 10000 rpm), washed with distilled water and 95% ethanol several times, and dried at 80 °C for 24 h in oven.

Characterization

The phase purity of the obtained products was analyzed by powder XRD by using a Bruker AXS D8 advanced automatic diffractometer with $Cu_{K\alpha}$ radiation (λ = 1.5405 Å, 40 kV 20 mA). The morphology and composition of the samples were inspected by using a field-emission gun transmission electron microscope (FEGTEM; JEM-2100F, JEOL) with a Link ISIS 300 EDX analyzer. The SAED patterns were obtained by using a FEGTEM instrument operating at 200 kV. The particle size of the products were analyzed by means of a Brookhaven 90 plus DLS particle size analyzer equipped with a 35 mW He–Ne laser. DLS measurement was carried out at a wavelength of λ = 632.8 nm at 25 °C with a 90° angle of detection. The PL/PL excitation (PLE) spectra were recorded on a Spex FluoroLog-3 spectrofluorometer equipped with a 450 W Xe lamp and cutoff filters to avoid second-order emissions of the source radiation. The conjugations of biomolecules with NCs were confirmed by MALDI-TOF mass spectrometry (Bruker Biflex III) and FTIR spectroscopy (Nicolet Avatar 320).

Conjugation of NCs with Biomolecules

FA (10 mg) was dissolved in dimethylsulfoxide (DMSO; 1 mL), and reacted with EDC (50 mM) at pH 5.5 in MES (10 mM) buffer for 15 min, in the dark, at room temperature. Then Sulfo-NHS (100 mM) dissolved in MES buffer (pH 5.5) was added to EDC–FA and reacted for 15 min in the dark, at room temperature. After incubation, the amino group modified YVO_4:Bi^{3+}, Eu^{3+} NCs were added to the mixture and reacted for 24 h in the dark at room temperature under vigorous shaking. Unconjugated FA and impurities were removed by centrifugation and the products were washed with distilled water and phosphate buffer solution (PBS) several times. EGF was also conjugated with the amino group modified YVO_4:Bi^{3+}, Eu^{3+} NCs by a similar procedure. The amino group modified YVO_4:Bi^{3+},Eu^{3+} NCs were reacted with recombinant human EGF with a molar ratio of 1:5:10 for EGF/EDC/NHS and the reaction proceeded for 2 h at room temperature. Unconjugated EGF and impurities were removed by centrifugation, and the EGF–YVO_4 NCs products were washed with distilled water and PBS buffer several times. The successful conjugation of FA with BPEI-coated YVO_4:Bi^{3+},Eu^{3+} NCs was confirmed by using FTIR spectroscopy by recording the absorbance of samples supported on KBr pellets in the frequency range from $\tilde{\nu}$ = 4000 to 450 cm^{-1}. The amount of sample in the KBr pellets was in the range of 0.2 to 1 wt%. The conjugation of EGF with BPEI-coated YVO_4:Bi^{3+},Eu^{3+} NCs was analyzed by MALDI-TOF MS. The samples were incubated overnight with trypsin (trypsin/protein 1:20) at 37 °C. A spot of α-cyano-4-hydroxycinnamic acid matrix (0.5 μL; 20 mg mL^{-1} in 50% HPLC grade acetonitrile, 0.1% trifluoroacetic acid (TFA)) was placed on a MALDI sample plate followed by 0.5 μL of sample (before/after trypsin digestion), dried, and then analyzed by using an autoflex III MALDI-TOF mass spectrometer (Bruker).

Cell Culture and Cellular Uptake

HeLa and A431 cells were purchased from the Culture Collection and Research Center (Hsinchu, Taiwan). The cells were cultured in RPMI1640 medium and Dulbeco's modified Eagle medium (DMEM) containing 10% fetal bovine serum (FBS) at 37 °C under 5% CO_2. The biomolecule-modified NCs were dispersed in cell culture medium with different concentrations ranging from 0.06 to 0.24 mg mL^{-1}. The NCs were incubated with cancer cells at 37 °C under 5% CO_2 for 2–4 h. After incubation, the cells were washed with PBS buffer to remove unbound NCs and fluorescence imaging was detected by using a Nikon TE2000-U fluorescent microscope under UV (λ = 330–380 nm) excitation. As a control, the pure NCs were incubated with cancer cells under the same experimental conditions.

Cell Cytotoxicity Assay

In vitro cytotoxicity of BPEI-coated YVO_4:Bi^{3+},Eu^{3+} NCs was assessed by means of an MTT assay kit. The cells were treated with different concentrations (0.1, 0.2, and 0.5 mg mL^{-1}) of NCs and maintained in a humidified atmosphere that consisted of 5% CO_2 in air at 37 °C for 2, 12, and 24 h. At the end of the incubation, MTT was added to each well and cells were incubated for another 4 h. All of the culture medium was removed carefully and DMSO was added to each well. The absorbance at λ = 570 nm was measured by a microplate reader. The viability data were compared with the numbers of cells in the untreated cultures and expressed as means and standard deviations from the three independent experiments.

Acknowledgements

This research was supported by the National Science Council of Taiwan (R.O.C.) under contract no. NSC 101-2113M-009-021-MY3. We thank Dr. Cheng Hsiang Chang and Dr. Wen Hung Chen for assistance with helpful suggestions.

[1] A. Jemal, R. Siegel, J. Xu, E. Ward, *Ca-Cancer J. Clin.* **2010**, *60*, 277–300.

[2] a) Y. Namiki, T. Fuchigami, N. Tada, R. Kawamura, S. Matsunuma, Y. Kitamoto, M. Nakagawa, *Acc. Chem. Res.* **2011**, *44*, 1080–1093; b) J. Shi, H. Zhang, L. Wang, L. Li, H. Wang, Z. Wang, Z. Li, C. Chen, L. Hou, C. Zhang, Z. Zhang, *Biomaterials* **2013**, *34*, 251–261; c) C. Zhang, C. Li, S. Huang, Z. Hou, Z. Cheng, P. Yang, C. Peng, J. Lin, *Biomaterials* **2010**, *31*, 3374–3383; d) C. Wang, L. Cheng, Z. Liu, *Biomaterials* **2011**, *32*, 1110–1120.

[3] a) H.-C. Lin, H.-H. Lin, C.-Y. Kao, A. L. Yu, W.-P. Peng, C.-H. Chen, *Angew. Chem.* **2010**, *122*, 3538–3542; *Angew. Chem. Int. Ed.* **2010**, *49*, 3460–3464; b) J. Chen, J. X. Zhao, *Sensors* **2012**, *12*, 2414–2435; c) H. S. Mader, O. S. Wolfbeis, *Anal. Chem.* **2010**, *82*, 5002–5004; d) D. E. Achatz, R. J. Meier, L. H. Fischer, O. S. Wolfbeis, *Angew. Chem.* **2011**, *123*, 274–277; *Angew. Chem. Int. Ed.* **2011**, *50*, 260–263; e) Z. Li, X. Wang, G. Wen, S. Shuang, C. Dong, M. C. Paau, M. M. F. Choi, *Biosens. Bioelectron.* **2011**, *26*, 4619–4623; f) Q. Yang, X. Gong, T. Song, J. Yang, S. Zhu, Y. Li, Y. Cui, Y. Li, B. Zhang, J. Chang, *Biosens. Bioelectron.* **2011**, *30*, 145–150.

[4] a) T. Maldiney, A. Lecointre, B. Viana, A. Bessière, M. Bessodes, D. Gourier, C. Richard, D. Scherman, *J. Am. Chem. Soc.* **2011**, *133*, 11810–11815; b) X. Li, L. Qiu, P. Zhu, X. Tao, T. Imanaka, J. Zhao, Y. Huang, Y. Tu, X. Cao, *Small* **2012**, *8*, 2505–2514.

[5] a) A. R. Bayles, H. S. Chahal, D. S. Chahal, C. P. Goldbeck, B. E. Cohen, B. A. Helms, *Nano Lett.* **2010**, *10*, 4086–4092; b) S. Reji-

nold N, K. P. Chennazhi, H. Tamura, S. V. Nair, J. Rangasamy, *ACS Appl. Mater. Interfaces* **2011**, *3*, 3654–3665; c) H.-M. Fan, M. Olivo, B. Shuter, J.-B. Yi, R. Bhuvaneswari, H.-R. Tan, G.-C. Xing, C.-T. Ng, L. Liu, S. S. Lucky, B.-H. Bay, J. Ding, *J. Am. Chem. Soc.* **2010**, *132*, 14803–14811.

[6] a) C. Kirchner, T. Liedl, S. Kudera, T. Pellegrino, A. Muñoz Javier, H. E. Gaub, S. Stölzle, N. Fertig, W. J. Parak, *Nano Lett.* **2005**, *5*, 331–338; b) A. M. Derfus, W. C. W. Chan, S. N. Bhatia, *Nano Lett.* **2004**, *4*, 11–18; c) M. J. D. Clift, C. Brandenberger, B. Rothen-Rutishauser, D. M. Brown, V. Stone, *Toxicology* **2011**, *286*, 58–68; d) W.-H. Chan, N.-H. Shiao, P.-Z. Lu, *Toxicol. Lett.* **2006**, *167*, 191–200.

[7] a) G. Ren, S. Zeng, J. Hao, *J. Phys. Chem. C* **2011**, *115*, 20141–20147; b) P. Huang, D. Chen, Y. Wang, *J. Alloys Compd.* **2011**, *509*, 3375–3381; c) T. S. Atabaev, J. H. Lee, D.-W. Han, Y.-H. Hwang, H.-K. Kim, *J. Biomed. Mater. Res. A* **2012**, *100A*, 2287–2294; d) G. Chen, H. Qiu, R. Fan, S. Hao, S. Tan, C. Yang, G. Han, *J. Mater. Chem.* **2012**, *22*, 20190–20196; e) H. Jiang, G. Wang, W. Zhang, X. Liu, Z. Ye, D. Jin, J. Yuan, Z. Liu, *J. Fluoresc.* **2010**, *20*, 321–328.

[8] a) W. O. Gordon, J. A. Carter, B. M. Tissue, *J. Lumin.* **2004**, *108*, 339–342; b) B. K. Gupta, T. N. Narayanan, S. A. Vithayathil, Y. Lee, S. Koshy, A. L. M. Reddy, A. Saha, V. Shanker, V. N. Singh, B. A. Kaipparettu, A. A. Martí, P. M. Ajayan, *Small* **2012**, *8*, 3028–3034.

[9] V. Buissette, D. Giaume, T. Gacoin, J.-P. Boilot, *J. Mater. Chem.* **2006**, *16*, 529–539.

[10] a) F. Wang, D. K. Chatterjee, Z. Li, Y. Zhang, X. Fan, M. Wang, *Nanotechnology* **2006**, *17*, 5786; b) S. Setua, D. Menon, A. Asok, S. Nair, M. Koyakutty, *Biomaterials* **2010**, *31*, 714–729; c) J. Jin, Y.-J. Gu, C. W.-Y. Man, J. Cheng, Z. Xu, Y. Zhang, H. Wang, V. H.-Y. Lee, S. H. Cheng, W.-T. Wong, *ACS Nano* **2011**, *5*, 7838–7847; d) J. Chen, C. Guo, M. Wang, L. Huang, L. Wang, C. Mi, J. Li, X. Fang, C. Mao, S. Xu, *J. Mater. Chem.* **2011**, *21*, 2632–2638; e) G. A. Sotiriou, D. Franco, D. Poulikakos, A. Ferrari, *ACS Nano* **2012**, *6*, 3888–3897; f) F. Zhang, S. S. Wong, *ACS Nano* **2010**, *4*, 99–112; g) B. K. Gupta, V. Rathee, T. N. Narayanan, P. Thanikaivelan, A. Saha, Govind, S. P. Singh, V. Shanker, A. A. Marti, P. M. Ajayan, *Small* **2011**, *7*, 1767–1773; h) N. Bogdan, E. M. Rodriguez, F. Sanz-Rodriguez, M. C. Iglesias de La Cruz, A. Juarranz, D. Jaque, J. G. Sole, J. A. Capobianco, *Nanoscale* **2012**, *4*, 3647–3650.

[11] a) J. Zhou, Z. Liu, F. Li, *Chem. Soc. Rev.* **2012**, *41*, 1323–1349; b) J.-C. G. Bünzli, *Chem. Rev.* **2010**, *110*, 2729–2755.

[12] a) J.-C. Boyer, F. C. J. M. van Veggel, *Nanoscale* **2010**, *2*, 1417–1419; b) G. Mialon, S. Türkcan, G. r. Dantelle, D. P. Collins, M. Hadjipanayi, R. A. Taylor, T. Gacoin, A. Alexandrou, J.-P. Boilot, *J. Phys. Chem. C* **2010**, *114*, 22449–22454.

[13] a) Z. Xu, X. Kang, C. Li, Z. Hou, C. Zhang, D. Yang, G. Li, J. Lin, *Inorg. Chem.* **2010**, *49*, 6706–6715; b) F. Wang, X. Xue, X. Liu, *Angew. Chem.* **2008**, *120*, 920–923; *Angew. Chem. Int. Ed.* **2008**, *47*, 906–909; c) E. Bauer, A. H. Mueller, I. Usov, N. Suvorova, M. T. Janicke, G. I. N. Waterhouse, M. R. Waterland, Q. X. Jia, A. K. Burrell, T. M. McCleskey, *Adv. Mater.* **2008**, *20*, 4704–4707; d) L. Li, M. Zhao, W. Tong, X. Guan, G. Li, L. Yang, *Nanotechnology* **2010**, *21*, 195601.

[14] S. Neeraj, N. Kijima, A. K. Cheetham, *Solid State Commun.* **2004**, *131*, 65–69.

[15] a) P. Scherrer, *Nachr. Ges. Wiss. Göttingen* **1918**, *2*, 98–100; b) W. C. Marra, P. Eisenberger, A. Y. Cho, *J. Appl. Phys.* **1979**, *50*, 6927–6933.

[16] K. Riwotzki, M. Haase, *J. Phys. Chem. B* **1998**, *102*, 10129–10135.

[17] Y. Wang, Y. Zuo, H. Gao, *Mater. Res. Bull.* **2006**, *41*, 2147–2153.

[18] a) Z. Xia, D. Chen, M. Yang, T. Ying, *J. Phys. Chem. Solids* **2010**, *71*, 175–180; b) D. Chen, Y. Yu, P. Huang, H. Lin, Z. Shan, L. Zeng, A. Yang, Y. Wang, *Phys. Chem. Chem. Phys.* **2010**, *12*, 7775–7778.

[19] a) O. Reelfs, Y.-Z. Xu, A. Massey, P. Karran, A. Storey, *Mol. Cancer Ther.* **2007**, *6*, 2487–2495; b) O. Reelfs, P. Karran, A. R. Young, *Photochem. Photobiol. Sci.* **2012**, *11*, 148–154.

[20] a) P. Rodighiero, A. Guiotto, A. Chilin, F. Bordin, F. Baccichetti, F. Carlassare, D. Vedaldi, S. Caffieri, A. Pozzan, F. Dall'Acqua, *J. Med. Chem.* **1996**, *39*, 1293–1302; b) J. J. Serrano-Pérez, M. Merchán, L. Serrano-Andrés, *J. Phys. Chem. B* **2008**, *112*, 14002–14010; c) J. A. Parrish, *J. Invest. Dermatol.* **1981**, *77*, 167.

[21] a) M. Arruebo, M. Valladares, A. González-Fernández, *J. Nanomaterials* **2009**, 439389; b) L. Wang, W. Su, Z. Liu, M. Zhou, S. Chen, Y. Chen, D. Lu, Y. Liu, Y. Fan, Y. Zheng, Z. Han, D. Kong, J. C. Wu, R. Xiang, Z. Li, *Biomaterials* **2012**, *33*, 5107–5114; c) R.-M. Lu, Y.-L. Chang, M.-S. Chen, H.-C. Wu, *Biomaterials* **2011**, *32*, 3265–3274.

[22] a) S. Jiang, Y. Zhang, K. M. Lim, E. K. W. Sim, L. Ye, *Nanotechnology* **2009**, *20*, 155101; b) S.-W. Tsai, J.-W. Liaw, F.-Y. Hsu, Y.-Y. Chen, M.-J. Lyu, M.-H. Yeh, *Sensors* **2008**, *8*, 6660–6673.

[23] a) D.-H. Yu, Q. Lu, J. Xie, C. Fang, H.-Z. Chen, *Biomaterials* **2010**, *31*, 2278–2292; b) H. Jin, J. Lovell, J. Chen, K. Ng, W. Cao, L. Ding, Z. Zhang, G. Zheng, *Cancer Nanotechnol.* **2010**, *1*, 71–78.

[24] a) L. Brannon-Peppas, J. O. Blanchette, *Adv. Drug Delivery Rev.* **2004**, *56*, 1649–1659; b) X. Qiang, T. Wu, J. Fan, J. Wang, F. Song, S. Sun, J. Jiang, X. Peng, *J. Mater. Chem.* **2012**, *22*, 16078–16083; c) E.-Q. Song, Z.-L. Zhang, Q.-Y. Luo, W. Lu, Y.-B. Shi, D.-W. Pang, *Clin. Chem.* **2009**, *55*, 955–963; d) L. Danglot, M. Chaineau, M. Dahan, M.-C. Gendron, N. Boggetto, F. Perez, T. Galli, *J. Cell Sci.* **2010**, *123*, 723–735; e) A. Antony, *Blood* **1992**, *79*, 2807–2820.

[25] S. Kobayashi, K. Hiroishi, M. Tokunoh, T. Saegusa, *Macromolecules* **1987**, *20*, 1496–1500.

[26] a) J. Intra, A. K. Salem, *J. Controlled Release* **2008**, *130*, 129–138; b) M. Günther, J. Lipka, A. Malek, D. Gutsch, W. Kreyling, A. Aigner, *Eur. J. Pharm. Biopharm.* **2011**, *77*, 438–449; c) J. M. Rosenholm, A. Meinander, E. Peuhu, R. Niemi, J. E. Eriksson, C. Sahlgren, M. Lindén, *ACS Nano* **2009**, *3*, 197–206; d) J. Cui, H. Cui, Y. Wang, C. Sun, K. Li, H. Ren, W. Du, *Adv. Mater. Sci. Eng.* **2012**, 764521.

[27] a) Y. C. Chen, Y. C. Wu, D. Y. Wang, T. M. Chen, *J. Mater. Chem.* **2012**, *22*, 7961–7969; b) K. Riwotzki, M. Haase, *J. Phys. Chem. B* **2001**, *105*, 12709.

[28] D. K. Chatterjee, A. J. Rufaihah, Y. Zhang, *Biomaterials* **2008**, *29*, 937–943.

[29] a) K. K. Comfort, E. I. Maurer, L. K. Braydich-Stolle, S. M. Hussain, *ACS Nano* **2011**, *5*, 10000–10008; b) Q. Yuan, E. Lee, W. A. Yeudall, H. Yang, *Oral Oncol.* **2010**, *46*, 698–704.

[30] a) T. J. Griffin, L. M. Smith, *Trends Biotechnol.* **2000**, *18*, 77–84; b) S. Kull, D. Pauly, B. Störmann, S. Kirchner, M. Stämmler, M. B. Dorner, P. Lasch, D. Naumann, B. G. Dorner, *Anal. Chem.* **2010**, *82*, 2916–2924; c) Z.-P. Yao, P. A. Demirev, C. Fenselau, *Anal. Chem.* **2002**, *74*, 2529–2534.

Received: April 24, 2013
Revised: May 22, 2013
Published online: July 24, 2013